

On the Optimal Radius and Subcarrier Mapping for Binary Modulation on Conjugate-Reciprocal Zeros

Parker Huggins

Department of Electrical Engineering
University of South Carolina
Columbia, SC, USA
parkerkh@email.sc.edu

Alphan Şahin

Department of Electrical Engineering
University of South Carolina
Columbia, SC, USA
asahin@mailbox.sc.edu

Abstract—In this work, we investigate the radius maximizing reliability for binary modulation on conjugate-reciprocal zeros (BMO CZ) implemented with both maximum likelihood (ML) and direct zero-testing (DiZeT) decoders. We first show that the optimal radius for BMO CZ is a function of the employed decoder and that the radius maximizing the minimum distance between polynomial zeros does not maximize the minimum distance of the final code. While maximizing zero separation offers an almost optimal solution with the DiZeT decoder, simulations show that the ML decoder outperforms the DiZeT decoder in both additive white Gaussian noise (AWGN) and fading channels when the radius is chosen to maximize codeword separation. Finally, we analyze different sequence-to-subcarrier mappings for BMO CZ-based orthogonal frequency division multiplexing (OFDM). We highlight a flexible time-frequency OFDM waveform that avoids distortion introduced by a frequency-selective channel at the expense of a higher peak-to-average power ratio (PAPR).

Index Terms—Huffman sequences, BMO CZ, polynomial zeros, OFDM, subcarrier mappings, waveforms.

I. INTRODUCTION

The emergence of the Internet-of-Things (IoT) has presented an abundance of challenges to modern communication systems. Unlike previous generations of cellular networks focused on enhancing spectral efficiency and data rate for human users, Fifth Generation (5G) New Radio (NR) has called for the development of novel use cases, including machine-type [1] and ultra-reliable low-latency communication [2]. To connect users, sensors, and devices on an unprecedented scale, these new demands necessitate flexible communication technologies that are adaptable to different environments. Moreover, the sparsity of the IoT motivates communication via the frequent transmission of sporadic short-packets [3], a type of communication whose architecture fundamentally differs from those used today [4].

Looking towards sixth-generation wireless networks, non-coherent communication strategies have gained traction for their ability to scale with the anticipated stark increase in wireless connectivity [5]. Furthermore, the low complexity and low power consumption of non-coherent based communication hardware lends itself to application in the IoT [6], where the billions of devices connected worldwide will pose challenges to current communication infrastructure. A non-coherent communication system is one in which the receiver has no explicit knowledge of channel state information (CSI).

In this case, equalization techniques that are commonplace in modern wireless communication systems cannot be used for symbol detection; rather, the receiver must perform “blind” demodulation of the received signal. The design of non-coherent communication systems that are both reliable and practical thus proves challenging [7].

A recently proposed non-coherent communication scheme for short packets is modulation on conjugate-reciprocal zeros (MOCZ). Using MOCZ, information bits are encoded into the zeros of the baseband signal’s z -transform. The baseband signal in the z -domain thus takes the form of a polynomial, and the transmitted sequence comprises the coefficients of this polynomial [8]. A particular advantage of MOCZ is that the polynomial zeros are unaffected by the channel impulse response (CIR). This is because the convolution of the polynomial coefficients with the CIR corresponds to multiplication in the z -domain, an operation that may introduce extraneous zeros to the received polynomial sequence but not alter those already transmitted [9]. Both the theoretical and practical aspects of MOCZ are studied extensively in [9] and [10]. In particular, a variant of MOCZ is introduced whereby each information bit is encoded into the zero of a conjugate-reciprocal zero pair. The technique is termed binary modulation on conjugate-reciprocal zeros (BMO CZ) and it yields polynomial coefficients that are Huffman sequences [11]. Furthermore, various improvements and applications of MOCZ have been considered in the literature. For example, the authors in [12] propose spectrally-efficient BMO CZ using faster-than-Nyquist signaling. In [13], codebooks are introduced for MOCZ that reduce peak-to-average power ratio (PAPR). In [14] and [15], the authors investigate diversity techniques and multi-user access for MOCZ, respectively.

A crucial parameter in the design of BMO CZ is the radius giving the placement of conjugate-reciprocal zero pairs. The choice of this radius determines the separation between both zero-vectors and codewords, i.e., factors influencing the performance of the communication scheme. For this reason, the radius maximizing zero separation for BMO CZ was derived in [9] and introduced in conjunction with a direct zero-testing (DiZeT) decoder. To our knowledge, however, the optimal radius for BMO CZ in general is not addressed. In this preliminary work, we investigate the optimal radius for

BMOZC implemented using both maximum likelihood (ML) and DiZeT decoders. We show that the ML decoder outperforms the DiZeT decoder in both additive white Gaussian noise (AWGN) and fading channels for appropriate choices of the radius parameter. Moreover, the merits of different subcarrier mapping strategies for BMOZC-based orthogonal frequency division multiplexing (OFDM) are discussed. Simulations of the proposed OFDM waveforms in a fading channel demonstrate that a time-mapping approach achieves the best block error rate (BLER) performance at the expense of increased PAPR.

Notation: The set of complex numbers is denoted by \mathbb{C} , and the complex-conjugate of a complex number $z = a + jb$ is expressed as $z^* = a - jb$. We denote the Euclidean norm of a vector $\mathbf{v} \in \mathbb{C}^{N \times 1}$ as $\|\mathbf{v}\|_2 = \sqrt{\mathbf{v}^H \mathbf{v}}$. The probability of an event A given event B is denoted by $\Pr(A|B)$. The circularly symmetric complex normal distribution with zero-mean and variance σ^2 is expressed as $\mathcal{CN}(0, \sigma^2)$. The expected value of a random variable X is denoted by $\mathbb{E}[X]$.

II. PRELIMINARIES

This section reviews BMOZC and describes the two decoders considered in this work. To begin, consider a binary message $\mathbf{m} = (m_0, m_1, \dots, m_{K-1})$. Using BMOZC, the K message bits are modulated onto K distinct zeros according to

$$\alpha_k = \begin{cases} R e^{j2\pi \frac{k}{K}}, & m_k = 1 \\ \frac{1}{R} e^{j2\pi \frac{k}{K}}, & m_k = 0 \end{cases}, \quad (1)$$

where $k = 0, 1, \dots, K-1$ and $R > 1$ is a radius determining the distance between conjugate-reciprocal zero pairs. By the fundamental theorem of algebra, the K zeros define a polynomial of degree K , namely,

$$X(z) = x_K \prod_{k=0}^{K-1} (z - \alpha_k), \quad (2)$$

where $z \in \mathbb{C}$ and $x_K \neq 0$ is a scalar multiple that does not affect the zero locations of $X(z)$. In discrete-time, the baseband sequence to transmit comprises the $K+1$ polynomial coefficients of $X(z)$, i.e., $\mathbf{x} = (x_0, x_1, \dots, x_K)^T$. It is typical to choose x_K such that transmitted sequences are normalized with unit energy or, equivalently, such that $\|\mathbf{x}\|_2^2 = 1$.

For the duration of transmission, it is assumed that the channel is linear time-invariant (LTI) with an L -tap impulse response $\mathbf{h} = (h_0, h_1, \dots, h_{L-1})^T$. Using the convolution theorem, the received sequence $\mathbf{y} = (y_0, y_1, \dots, y_{K+L-1})^T$ can be expressed in the z -domain as

$$Y(z) = X(z)H(z) + W(z), \quad (3)$$

where $H(z)$ and $W(z)$ represent the unilateral z -transform of \mathbf{h} and a noise sequence $\mathbf{w} = (w_0, w_1, \dots, w_{K+L-1})^T$, respectively. Note that $H(z)$ and $W(z)$ are both polynomials in the complex variable z and thus can be factored in terms of their zeros. For $N = K + L$, we can write

$$H(z) = h_{L-1} \prod_{l=0}^{L-2} (z - \beta_l) \quad (4)$$

and

$$W(z) = w_{N-1} \prod_{n=0}^{N-2} (z - \gamma_n). \quad (5)$$

Therefore, the polynomial in (3) has a total of $N - 1$ zeros, K of which are information-bearing.

The authors in [9] propose several methods for demodulating and decoding the received polynomial sequence. In particular, introduced are an ML and DiZeT decoder. The ML decoder estimates the transmitted zeros by searching over all possible zero-vectors $\boldsymbol{\alpha} \in \mathcal{Z}^K$, where \mathcal{Z}^K is the BMOZC zero-codebook for a given K ; the codebook is generated by taking the Cartesian product of all conjugate-reciprocal zero pairs $\mathcal{Z}_k = \{\alpha_k, 1/\alpha_k^*\}$, i.e., $\mathcal{Z}^K = \mathcal{Z}_1 \times \mathcal{Z}_2 \times \dots \times \mathcal{Z}_K$. Using the ML decoder, assuming a uniform power-delay profile (PDP) [9], an estimate of the transmitted zeros is obtained directly as

$$\hat{\boldsymbol{\alpha}} = \arg \min_{\boldsymbol{\alpha} \in \mathcal{Z}^K} \left\| \left(\mathbf{V}_{\boldsymbol{\alpha}}^H \mathbf{V}_{\boldsymbol{\alpha}} \right)^{-\frac{1}{2}} \mathbf{V}_{\boldsymbol{\alpha}}^H \mathbf{y} \right\|_2^2, \quad (6)$$

where $\mathbf{V}_{\boldsymbol{\alpha}}^H$ is the $K \times N$ Vandermonde matrix

$$\mathbf{V}_{\boldsymbol{\alpha}}^H = \begin{pmatrix} 1 & \alpha_1 & \alpha_1^2 & \dots & \alpha_1^{N-1} \\ 1 & \alpha_2 & \alpha_2^2 & \dots & \alpha_2^{N-1} \\ \vdots & \vdots & \vdots & \ddots & \vdots \\ 1 & \alpha_K & \alpha_K^2 & \dots & \alpha_K^{N-1} \end{pmatrix}. \quad (7)$$

Instead of searching across all $\boldsymbol{\alpha} \in \mathcal{Z}^K$, the DiZeT decoder simply evaluates the received polynomial in (3) at the zeros in \mathcal{Z}_k . The k th transmitted zero is then estimated as

$$\hat{\alpha}_k = \arg \min_{\alpha_k \in \mathcal{Z}_k} R^{-\frac{N-1}{2}} |Y(\alpha_k)|, \quad (8)$$

where the weighting factor $R^{-(N-1)/2}$ is introduced to scale the output of $|Y(\alpha_k)|$ to balance the exponential nature of the polynomial coefficients [9].

III. DESIGN CONSIDERATIONS

A. Optimal Radius

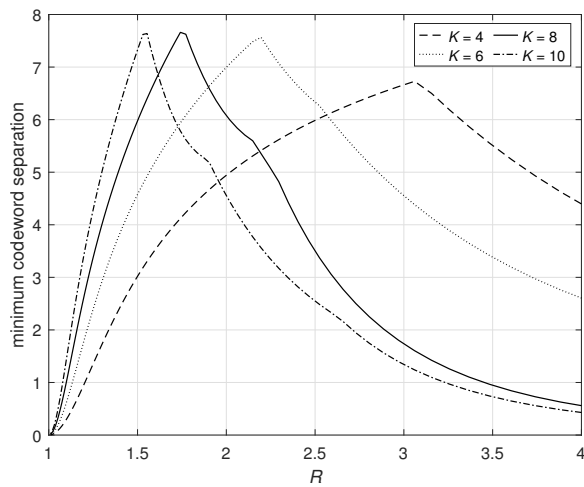
The form of (1) raises a natural question: for a given K , what is the radius R that maximizes the reliability of BMOZC? The accepted answer in current literature is the radius which maximizes the separation between zeros [9], [10], [12], i.e.,

$$R_{\text{DZ}}(K) = \sqrt{1 + \sin(\pi/K)}. \quad (9)$$

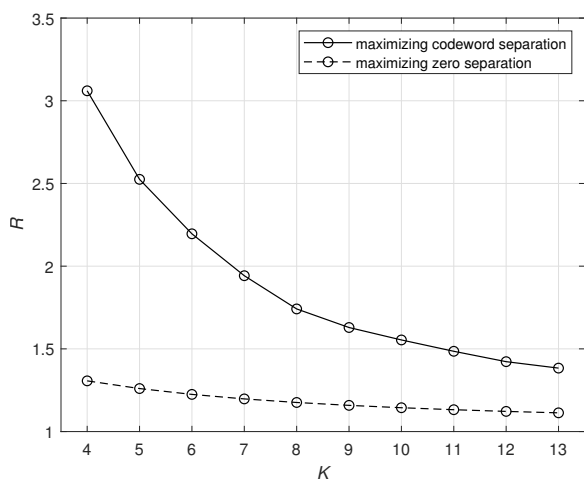
This result is intuitive for BMOZC employing the DiZeT decoder, for the received polynomial sequence is directly evaluated at the possible zero locations. The ML decoder, however, does not involve the explicit evaluation of (3) at any zeros. Moreover, the ML decoder is derived from the general maximum likelihood sequence estimator (MLSE) [16] given by

$$\hat{\mathbf{x}} = \arg \max_{\mathbf{x} \in \mathcal{C}^K} \Pr(\mathbf{y}|\mathbf{x}), \quad (10)$$

where \mathcal{C}^K is the BMOZC polynomial-codebook for a given K [9]. Since the optimization is performed over polynomial



(a) Minimum codeword separation against R values.



(b) Optimal R for various K values.

Fig. 1. Minimum codeword separation and the radii maximizing zero and codeword separation for select K .

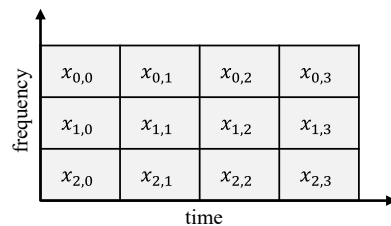
sequences and not zeros, it is best to choose the radius that maximizes the separation between codewords, i.e.,

$$R_{\text{ML}}(K) = \arg \max_{R>1} \left(\min_{\mathbf{x}_i, \mathbf{x}_j \in \mathcal{C}^K} \|\mathbf{x}_i - \mathbf{x}_j\|_2^2 \right), \quad i \neq j. \quad (11)$$

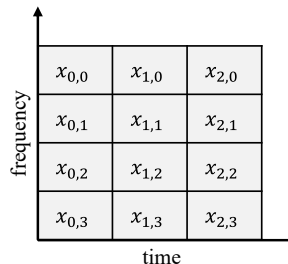
To compare the radii given in (9) and (11), we generate BMOZ zero- and polynomial-codebooks for various K . Fig. 1(a) displays the minimum observed codeword separation for $K \in \{4, 6, 8, 10\}$ and $R \in (1, 4]$. Fig. 1(b) shows the corresponding radii maximizing zero and codeword separation for $K \in \{4, 5, \dots, 13\}$, i.e., the radii computed in accordance with (9) and (11), respectively. For all K , notice that the radius maximizing codeword separation is greater than that maximizing zero separation. It follows that the optimal radius for BMOZ is a function of the utilized decoder.

B. OFDM Subcarrier Mappings

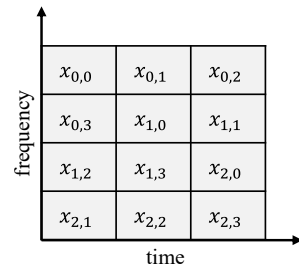
This section outlines how we construct BMOZ-based OFDM waveforms to limit the number of additional zeros



(a) Time-mapping.



(b) Frequency-mapping.



(c) Time-frequency mapping.

Fig. 2. Examples of the three principal sequence-to-subcarrier mappings for BMOZ-based OFDM with $P = 3$, $K = 3$, and $M = 3$.

in (3) introduced by the channel [15]. We begin by considering a binary message of length $B \geq K$. Next, P polynomials are generated by mapping every K bits of the message to sequences via BMOZ. Let $x_{p,k}$ denote the k th coefficient of the p th polynomial for $p \in \{0, 1, \dots, P-1\}$ and $k \in \{0, 1, \dots, K\}$. In principle, there exists three distinct sequence-to-subcarrier mappings: time-mapping, frequency-mapping, and time-frequency mapping. In what follows, we discuss the merits of each approach.

With time-mapping, P subcarriers are allocated for the polynomial sequences. The ℓ th subcarrier of $K+1$ OFDM symbols then constitutes one of the P polynomials. Specifically, the m th OFDM symbol can be expressed as

$$s_m[n] = \frac{1}{\sqrt{N_{\text{idft}}}} \sum_{\ell=0}^{\mathcal{L}-1} d_{\ell,m} e^{j2\pi\ell \frac{n}{N_{\text{idft}}}}, \quad -N_{\text{cp}} \leq n < N_{\text{idft}}, \quad (12)$$

where $d_{\ell,m}$ is the data symbol transmitted on the ℓ th subcarrier of the m th OFDM symbol, N_{idft} is the inverse discrete Fourier transform (IDFT) size, and N_{cp} is the cyclic prefix (CP) size. For time-mapping, $d_{\ell,m}$ is simply the k th polynomial coefficient of the p th polynomial sequence, i.e., $d_{\ell,m} = x_{p,k}$ for $\ell = p \in \{0, 1, \dots, P-1\}$ and $m = k \in \{0, 1, \dots, K\}$. Fig. 2(a) illustrates the time-mapping approach in the simple case where $P = K = 3$. The advantage of time-mapping is that it can accommodate large K , provided that the duration of each sequence is less than the coherence time of the channel. Moreover, even in a frequency-selective channel, each polynomial sequence experiences multiplication by a single complex gain due to the CP. Hence, no additional zeros are introduced to the transmitted sequences (i.e., $L_{\text{eff}} = 1$).

With frequency-mapping, the polynomial coefficients are mapped to subcarriers directly such that each OFDM symbol holds a single polynomial sequence, i.e., $\mathcal{L} = K + 1$ and

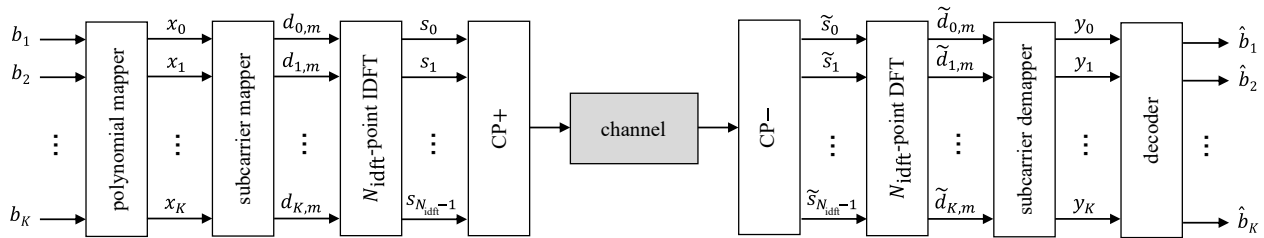


Fig. 3. Block diagram showing the processing of the m th OFDM symbol for a frequency-mapping approach ($m = p$).

$d_{\ell,m} = x_{p,k}$ for $\ell = k$ and $m = p$. A simple example of the frequency-mapping approach is provided in Fig. 2(b) for $P = K = 3$. Fig. 3 depicts the block diagram of a general BMOZ-based OFDM system implemented with frequency-mapping. Because Huffman sequences have almost ideal aperiodic auto-correlation functions [11], mapping the sequences to frequency and not time is beneficial for PAPR. However, the disadvantage of this approach is that coefficients of the same polynomial sequence can experience multiplication by different complex gains. The length of transmittable sequences is therefore limited by the coherence bandwidth of the channel, an imposition often much stricter than the coherence time in practice, particularly for low-mobility environments.

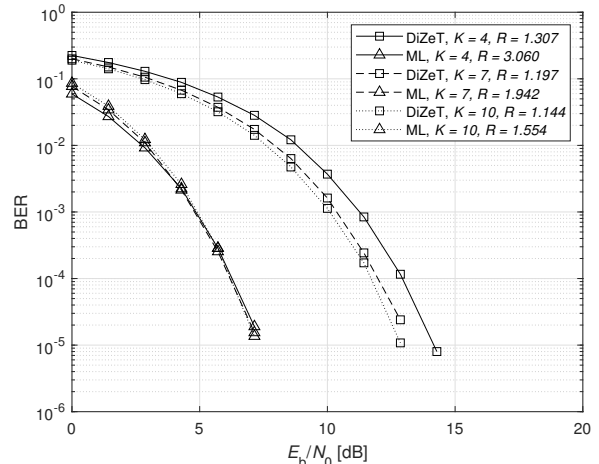
Time-frequency mapping utilizes M OFDM symbols and $\mathcal{L} = \lceil P(K+1)/M \rceil$ subcarriers. The data symbol transmitted on the ℓ th subcarrier of the m th OFDM symbol is $d_{\ell,m} = x_{p,k}$ for $p = \lfloor \frac{\ell M + m}{K+1} \rfloor$, $k = \text{mod}(\ell M + m, K+1)$, $\ell \in \{0, 1, \dots, \mathcal{L}-1\}$, and $m \in \{0, 1, \dots, M-1\}$. An example of time-frequency mapping is depicted in Fig. 2(c) for $M = 3$ and $\mathcal{L} = 4$. The advantage of time-frequency mapping is its flexibility, for either the number of OFDM symbols or subcarriers can be freely selected. This is not the case for time- and frequency-mapping approaches where the number of OFDM symbols and the number of subcarriers is fixed to $K+1$, respectively.

IV. NUMERICAL RESULTS

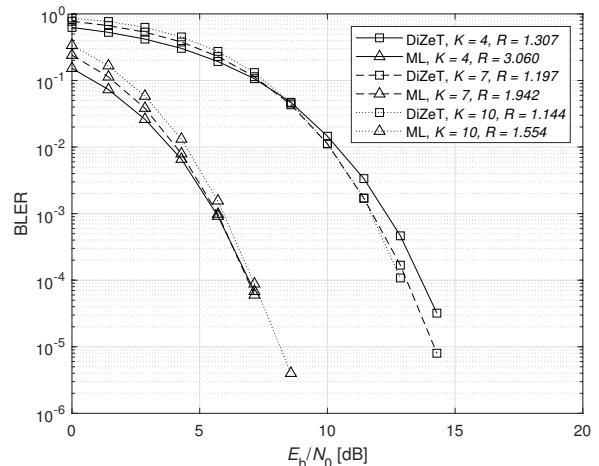
A. Decoder Performance at Optimal Radius

This section compares the performance of a BMOZ-based OFDM scheme for short-packet transmission implemented with frequency-mapping and both the ML and DiZeT decoders. We simulate the transmission of OFDM symbols through both an AWGN and fading channel. In the AWGN channel, signals are perturbed by a noise vector \mathbf{w} with elements drawn from a complex normal distribution having zero-mean and variance N_0 , i.e., $w_i \sim \mathcal{CN}(0, N_0)$. In the fading channel, subcarriers of the i th OFDM symbol are multiplied by the same single-tap complex gain $H_i \sim \mathcal{CN}(0, 1)$ before being perturbed by AWGN.¹ For each K , the IDFT size is $N_{\text{idft}} = 2^K$, and the radius used to generate codebooks is computed according to (9) and (11) for the DiZeT and ML decoders, respectively.

¹The authors note that because each subcarrier is multiplied by the same complex gain, $L = L_{\text{eff}} = 1$, and the performance of time- and frequency-mapping are rendered equivalent.



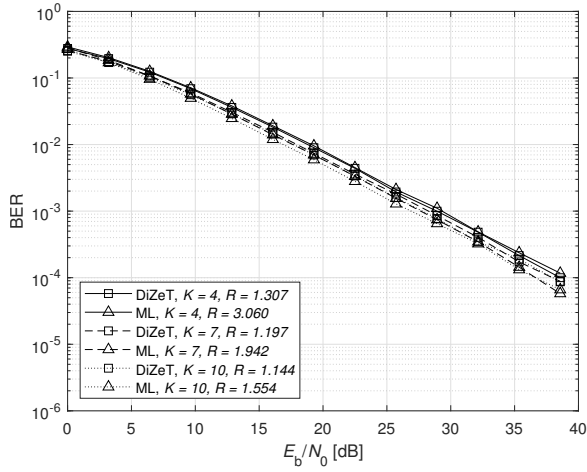
(a) Bit error rate performance in AWGN.



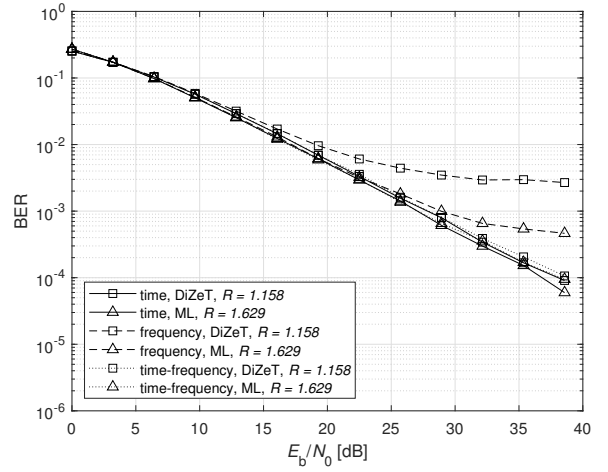
(b) Block error rate performance in AWGN.

Fig. 4. Comparison of the ML and DiZeT decoders in an AWGN channel. For each K , the radius R is chosen to maximize codeword and zero separation for the ML and DiZeT decoders, respectively.

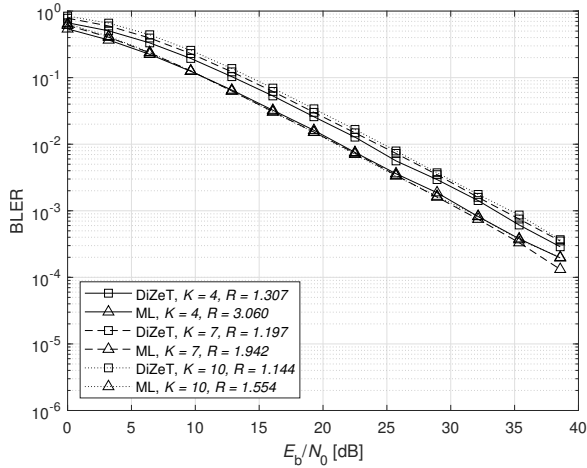
Fig. 4 shows the bit error rate (BER) and BLER curves simulated in the AWGN channel for BMOZ with $K \in \{4, 7, 10\}$. The ML decoder outperforms the DiZeT decoder in terms of both BER and BLER by a margin greater than 5 dB. This result is expected as the polynomial coefficients of BMOZ are more robust against additive noise than the zeros [9], [17]. Fig. 5 pictures the BER and BLER curves simulated in the fading channel for BMOZ with $K \in \{4, 7, 10\}$. While the BER



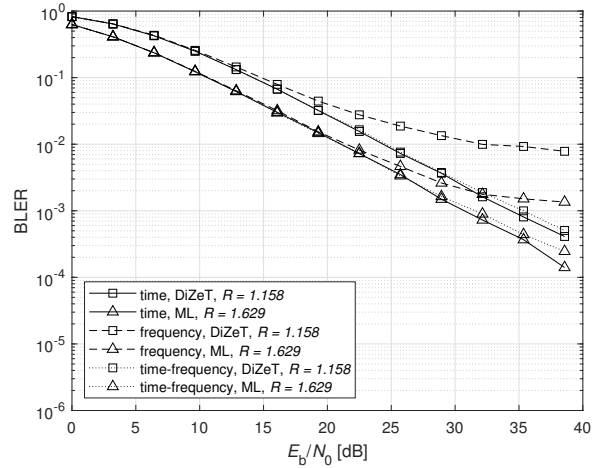
(a) Bit error rate performance in a fading channel.



(a) Bit error rate performance in a fading channel.



(b) Block error rate performance in a fading channel.



(b) Block error rate performance in a fading channel.

Fig. 5. Comparison of the ML and DiZeT decoders in a fading channel with $L = 1$. For each K , the radius R is chosen to maximize codeword and zero separation for the ML and DiZeT decoders, respectively.

Fig. 6. Comparison of the OFDM subcarrier mappings in a fading channel for $L = K = 9$ and $\rho = 0.2$. The radius R is chosen to maximize codeword and zero separation for the ML and DiZeT decoders, respectively.

performance of the two decoders is comparable, notice that the ML decoder again outperforms the DiZeT decoder in BLER, this time by a margin of roughly 3 dB. Thus, for suitable choices of the radius R , the ML decoder achieves more reliable communication than the DiZeT decoder for BMOZC.

B. Error Rates for Different Subcarrier Mappings

This section compares the performance of the OFDM subcarrier mappings in a fading channel. We consider a decaying exponential power-delay profile (PDP) having L taps given by

$$\rho_l = \mathbb{E}[|h_l|^2] = \frac{1-\rho}{1-\rho^L} \rho^l, \quad (13)$$

where $l \in \{0, 1, \dots, L-1\}$ and $\rho \in (0, 1)$ is the profile's decay constant [9]. Simulations are performed with packets comprising $P = 64$ polynomial sequences, $L = K = 9$, $N_{\text{idft}} = 256$, and $\rho = 0.2$. The number of OFDM symbols and subcarriers considered for time-frequency mapping is $M = 5$ and $\mathcal{L} = 128$, respectively. For the DiZeT and ML

decoders, we again generate BMOZC codebooks using the corresponding radii in (9) and (11).

Fig. 6 shows the BER and BLER curves of the three OFDM waveforms simulated in the fading channel. As anticipated from the discussion in III-B, the time-mapping waveform outperforms the frequency-mapping waveform as each polynomial sequence observes flat-fading. In fact, the waveform with frequency-mapping experiences an error floor due to distortion of the polynomial coefficients induced by the frequency-selective channel. It can be seen that time-frequency mapping performs similarly to time-mapping. Given its heightened flexibility, however, we regard the time-frequency waveform as the most practical for real implementations, provided that PAPR is not a primary design constraint.

C. PAPR for Different Subcarrier Mappings

In this section, we compare the PAPR of the described subcarrier mappings for BMOZC-based OFDM. The PAPR

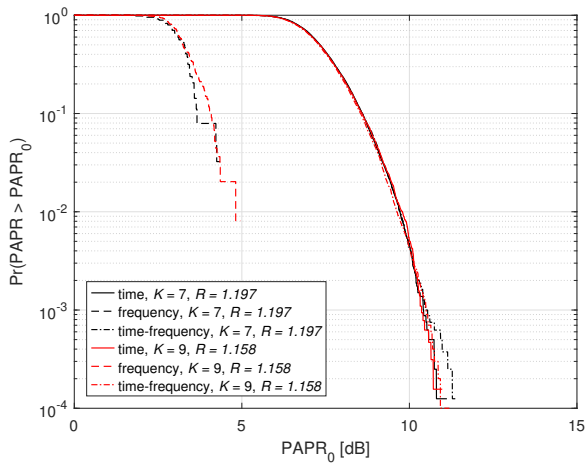


Fig. 7. CCDF of PAPR for BMOZ-based OFDM waveforms employing different sequence-to-subcarrier mappings.

of a discrete-time signal $s[n]$ with length N_s is computed as

$$\text{PAPR}(s[n])_{\text{dB}} = 10 \log_{10} \left(\frac{\max |s[n]|^2}{P_{\text{avg}}} \right), \quad (14)$$

where P_{avg} is the average power of the signal, i.e.,

$$P_{\text{avg}} = \frac{1}{N_s} \sum_{n=0}^{N_s-1} |s[n]|^2. \quad (15)$$

For our simulations, a single packet consists of $P = 64$ polynomial sequences. The IDFT size for each mapping strategy is $N_{\text{idft}} = 512$, and a quadrature phase-shift keying (QPSK) scrambler is implemented for time-mapping and time-frequency mapping to reduce PAPR. Fig. 7 shows the complementary cumulative distribution function (CCDF) of PAPR computed for $K \in \{7, 9\}$ and the radius R from (11). While there appears no considerable difference between PAPR for time-mapping and time-frequency mapping, PAPR is indeed minimized by mapping the polynomial sequences directly to frequency.

V. CONCLUDING REMARKS

In this work, we investigate the radius for BMOZ that maximizes communication reliability. We first show that different radii maximize zero and codeword separation and that the optimal radius for BMOZ is a function of the utilized decoder (i.e., ML or DiZeT). Simulations of a BMOZ-based OFDM waveform in AWGN and fading channels validate that the ML decoder outperforms the DiZeT decoder for suitable choices of the radius parameter. Finally, we discuss the merits of different sequence-to-subcarrier mappings for BMOZ-based OFDM to limit the number of zeros introduced by the channel. We

propose a flexible time-frequency mapping approach that is robust against a frequency-selective channel at the expense of increased PAPR. Future work will focus on the optimal radius for MOCZ more generally, the derivation of an expression for the radius maximizing codeword separation, and further quantitative analysis of the introduced BMOZ-based OFDM waveforms.

REFERENCES

- [1] C. Bockelmann, N. Pratas, H. Nikopour, K. Au, T. Svensson, C. Stefanovic, P. Popovski, and A. Dekorsy, "Massive machine-type communications in 5G: Physical and MAC-layer solutions," *IEEE Communications Magazine*, vol. 54, no. 9, pp. 59–65, 2016.
- [2] P. Popovski, "Ultra-reliable communication in 5G wireless systems," in *Proc. 1st International Conference on 5G for Ubiquitous Connectivity*. IEEE, 2014, pp. 146–151.
- [3] G. Wunder, H. Boche, T. Strohmer, and P. Jung, "Sparse signal processing concepts for efficient 5G system design," *IEEE Access*, vol. 3, pp. 195–208, 2015.
- [4] X. You, C.-X. Wang, J. Huang, X. Gao, Z. Zhang, M. Wang, Y. Huang, C. Zhang, Y. Jiang, J. Wang *et al.*, "Towards 6G wireless communication networks: Vision, enabling technologies, and new paradigm shifts," *Science China Information Sciences*, vol. 64, pp. 1–74, 2021.
- [5] S. J. Nawaz, S. K. Sharma, B. Mansoor, M. N. Patwary, and N. M. Khan, "Non-coherent and backscatter communications: Enabling ultra-massive connectivity in 6G wireless networks," *IEEE Access*, vol. 9, pp. 38 144–38 186, 2021.
- [6] K. Witrisal, G. Leus, G. J. Janssen, M. Pausini, F. Trösch, T. Zasowski, and J. Romme, "Noncoherent ultra-wideband systems," *IEEE Signal Processing Magazine*, vol. 26, no. 4, pp. 48–66, 2009.
- [7] C. Xu, N. Ishikawa, R. Rajashekar, S. Sugiura, R. G. Maunder, Z. Wang, L.-L. Yang, and L. Hanzo, "Sixty years of coherent versus non-coherent tradeoffs and the road from 5G to wireless futures," *IEEE Access*, vol. 7, pp. 178 246–178 299, 2019.
- [8] P. Walk, P. Jung, and B. Hassibi, "Short-message communication and FIR system identification using Huffman sequences," in *Proc. IEEE International Symposium on Information Theory (ISIT)*. IEEE, 2017, pp. 968–972.
- [9] —, "MOCZ for blind short-packet communication: Basic principles," *IEEE Transactions on Wireless Communications*, vol. 18, no. 11, pp. 5080–5097, 2019.
- [10] P. Walk, P. Jung, B. Hassibi, and H. Jafarkhani, "MOCZ for blind short-packet communication: Practical aspects," *IEEE Transactions on Wireless Communications*, vol. 19, no. 10, pp. 6675–6692, 2020.
- [11] M. H. Ackroyd, "The design of Huffman sequences," *IEEE Transactions on Aerospace and Electronic Systems*, no. 6, pp. 790–796, 1970.
- [12] A. A. Siddiqui, E. Bedeer, H. H. Nguyen, and R. Barton, "Spectrally-efficient modulation on conjugate-reciprocal zeros (SE-MOCZ) for non-coherent short packet communications," *IEEE Transactions on Wireless Communications*, 2023.
- [13] B. Sasidharan, E. Viterbo, and Y. Hong, "Alternative zero codebooks for MOCZ with reduced PAPR," *IEEE Communications Letters*, 2024.
- [14] Y. Sun, Y. Zhang, G. Dou, Y. Lu, and Y. Song, "Noncoherent SIMO transmission via MOCZ for short packet-based machine-type communications in frequency-selective fading environments," *IEEE Open Journal of the Communications Society*, 2023.
- [15] P. Walk and W. Xiao, "Multi-user MOCZ for mobile machine type communications," in *Proc. IEEE Wireless Communications and Networking Conference (WCNC)*. IEEE, 2021, pp. 1–6.
- [16] G. Forney, "Maximum-likelihood sequence estimation of digital sequences in the presence of intersymbol interference," *IEEE Transactions on Information Theory*, vol. 18, no. 3, pp. 363–378, 1972.
- [17] J. H. Wilkinson, "The perfidious polynomial," *Studies in Numerical Analysis*, vol. 24, pp. 1–28, 1984.